

NJC

Accepted Manuscript



This is an *Accepted Manuscript*, which has been through the Royal Society of Chemistry peer review process and has been accepted for publication.

Accepted Manuscripts are published online shortly after acceptance, before technical editing, formatting and proof reading. Using this free service, authors can make their results available to the community, in citable form, before we publish the edited article. We will replace this *Accepted Manuscript* with the edited and formatted *Advance Article* as soon as it is available.

You can find more information about *Accepted Manuscripts* in the [Information for Authors](#).

Please note that technical editing may introduce minor changes to the text and/or graphics, which may alter content. The journal's standard [Terms & Conditions](#) and the [Ethical guidelines](#) still apply. In no event shall the Royal Society of Chemistry be held responsible for any errors or omissions in this *Accepted Manuscript* or any consequences arising from the use of any information it contains.



www.rsc.org/njc



Journal Name

ARTICLE

The conformational behaviour of naproxen and flurbiprofen in solution by NMR spectroscopy

Maria Enrica Di Pietro,^{a,*} Christie Aroulanda,^b Giorgio Celebre,^a Denis Merlet,^{b,*} and Giuseppina De Luca^{a,*}

Received 00th January 20xx,
Accepted 00th January 20xx

DOI: 10.1039/x0xx00000x

www.rsc.org/

Naproxen and flurbiprofen are among the most popular and widely used drugs for treating pain and inflammation and new different therapeutic uses are still proposed. Their pharmacological activity comes from the specific binding to target proteins and is evidently driven by the spatial arrangement they adopt at the active sites. A detailed conformational analysis in solution able to probe equilibria between more possible conformers is then crucial for understanding and rationalizing their biological role and possibly for designing improved analogues. Here we combine NMR data obtained in weakly ordering media and suitable theoretical models to look for the energetically-admissible conformers of these two anti-inflammatory drugs in a liquid medium. This approach leads to rather complex probability distributions characterized for both molecules by an equilibrium of different global and local minimum energy structures.

Introduction

Naproxen (2-(6-methoxy-2-naphthalen)propanoic acid) and flurbiprofen (2-(2-fluoro-4-biphenyl)propanoic acid) are two popular non-steroidal anti-inflammatory drugs (NSAIDs) belonging to the family of 2-arylpropionic acids, commonly known as profens. Profens are among the most important drugs in common use, both economically and clinically, and are widely employed as therapeutic agents for the treatment of pain and inflammation. Their anti-inflammatory and antipyretic action as well as the side-effects like gastrointestinal irritation are based on the nonselective blockage of the two known isoforms of prostaglandin H₂ synthase enzyme (PGHS, also known as cyclooxygenase, COXs)¹ with following inhibition of downstream prostanoid species.²⁻³ Profens are chiral molecules and individual enantiomers differ in their pharmacological activity.⁴⁻⁵ *In vitro* and *in vivo* studies demonstrated that the anti-inflammatory activity due to COX inhibition is largely stereospecific for the *S*-enantiomers.⁶ More recent works proved *R*-isomers can have different appealing activities thanks to alternative binding modes to COX enzymes⁷ or inhibition of non-conventional targets.⁸

S-naproxen is one of the oldest and most largely sold NSAIDs, it is widely used in the treatment of many inflammatory diseases⁹ and it has been reported to be effective in the treatment of migraine-

associated symptoms.¹⁰ According to various studies, naproxen is a promising candidate for chemoprevention¹¹ and its long-term prophylactic use might reduce the risk of Alzheimer disease.¹²⁻¹³ The *S*-enantiomer of naproxen is 28-fold more active as anti-inflammatory than the *R*-isomer,¹⁴ which is reported to be a liver toxin¹⁵ and to incidentally cause gastrointestinal disorders.¹⁶ Hence, to date naproxen and its sodium salt have been internationally delivered as the pure *S*-(+)-isomers. Their crystal structures have been determined by X-ray measurements¹⁷⁻¹⁸ and computer modelling for crystal structure prediction found very different crystal packing for the enantiomeric and racemic form.¹⁹

Unlike naproxen, flurbiprofen has been traditionally marketed as racemic mixtures. Although the anti-inflammatory activity is almost entirely attributable to *S*-flurbiprofen,²⁰ and in humans *R*-flurbiprofen undergoes very limited chiral inversion to the *S*-enantiomer,²¹ both enantiomers have been shown to exhibit antinociceptive activity²² and antiproliferative effects²³ with different mechanisms. In the last two decades, the *R*-enantiomer (often re-named Tarenflurbil) has been proposed as chemopreventive agent in pre-malignant hyperproliferative states, therapeutic agent for prostate cancer and adenocarcinoma, and as an anti-metastatic agent.²⁴⁻²⁶ Moreover it has been suggested as drug candidate for the treatment or prevention of Alzheimer's disease.²⁷ In both cases it appears to be well tolerated in humans and, when compared to the *S*-enantiomer, it can be administered in higher doses with a reduced toxicity, most frequently gastric ulceration, but also liver and kidney damage.²⁶

From these few examples it should be clear that the up-to-date knowledge on naproxen and flurbiprofen, their mechanisms of action, biochemical activities and side effects, cannot be considered exhaustive. Indeed, these drugs may bind different proteins with different mechanisms and orientations and new targets are likely to be individuated in the future. In general, when a given flexible

^a Lab. LXNMR, S.C.An., Dipartimento di Chimica e Tecnologie Chimiche, Università della Calabria, via P. Bucci, 87036, Arcavacata di Rende (CS), Italy, Fax: +39 0984493301; Tel: +39 0984493323/0984493320. E-mail: giuseppina.deluca@unical.it; mariaenrica.dipietro@unical.it

^b Equipe de RMN en milieu orienté, ICMMO, UMR 8182 CNRS, Université Paris-Sud, 15 rue Georges Clemenceau, 91405, Orsay, France, Fax: +33 0169158105; Tel: +33 0169157432. E-mail: denis.merlet@u-psud.fr

Electronic Supplementary Information (ESI) available: Tables listing experimental chemical shifts, scalar and total couplings for all samples; Experimental NMR spectra; Figures showing the relaxed PES scans obtained for NAP and FLU at DFT level; Tables with the geometries used in the conformational analysis; Tables reporting the optimised values of the iteration parameters used in the conformational analysis of NAP and FLU with the AP-DPD approach. See DOI: 10.1039/x0xx00000x

ligand binds to a receptor, and initiates then a biological effect, it has to adopt a conformation which is in some way complementary to its target protein. This protein-bound conformation is known as the bioactive conformation.²⁸ Intuitively the determination of the bioactive conformation of profens is an important challenge since it may help in gaining knowledge about the drug-protein complex, and thus be used as a template when designing novel anti-inflammatory agents with desired properties. However, the determination of the bioactive conformation is often far from being a trivial task. It has been observed that in lots of cases the bioactive conformation of a flexible ligand does not correspond to its global energy minimum in the free state²⁹ and lies instead at or very close to a local minimum on the potential energy surface (PES).²⁸ In addition, different receptors or receptor subtypes can bind the same drug in different conformations.³⁰ Another important point to consider is that the bioactive conformation of a molecule depends on its specific medium. It is a general assumption that the conformation in solution is similar to the bound conformation and is a better representation of the bioactive conformation than a structure individuated in the solid or gas state.³¹ This means that, for flexible compounds, structures experimentally determined by single crystal X-ray crystallography do not always well represent the protein-bound conformation in shape and are then less useful in the context of drug design than generally assumed.^{28,32} Similarly, the protein-bound structures of a flexible molecule often do not correlate well with the global minima found for an isolated molecule by *in vacuo* calculations and the correspondence is even worse for molecules able to form hydrogen bonds.³³⁻³⁴

An approach to solve the problem that ligand flexibility causes in drug design lies in the exploration of a wide conformational space highlighting all the possible minima that the molecule can assume. Indeed, when searching the bioactive conformations or the compounds fitting a pharmacophore and when examining the binding of a ligand to an enzyme, it is recommended to consider a more extended and diverse set of conformations rather than a single conformer.³² The exclusion of conformations that are physically impossible due to steric clashes between atoms and those strongly disfavoured energetically is entirely permissible, but restricting the study to the conformation measured in the isolated crystal or the global energy minimum calculated *in vacuo* is a treacherous practice.

In this sense, progress has been made in computer-aided drug design. A number of computational procedures, such as 3D-database searching, rigid-fit pharmacophore modeling, and docking studies, have been implemented where representative conformational series, *i.e.* those containing the bioactive conformation, are employed.²⁸ In these methods, multiple conformations of each potential ligand are evaluated, and their complementarity to the binding site of a given protein is estimated.²⁹

From the experimental point of view, solid-state NMR spectroscopy and X-ray crystallography are currently the techniques of choice for structure-based drug design.³⁴ However, they do not allow to probe molecular structure in solution, where the equilibrium between different possible conformers should be taken into account. NMR spectroscopy in solution may reveal useful in this respect. First, torsional

internal motions interconverting the possible conformers are rapid enough, on the NMR timescale, that the spectral parameters are averages over these motions. *Via* these average values, it is thus possible to investigate the molecular internal motions and then the flexibility of molecules. A second important point is that such investigation is performed in solution, which is closer to the physiological environment of bioactive molecules compared to solid or gas phase. To have access to such conformational information, an elegant tool is provided by the measurement of anisotropic residual dipolar couplings (RDCs) that affect the NMR spectra when solutes are dissolved in partially ordered media. It is widely shown in the literature³⁵⁻⁴¹ that RDCs represent richly informative probes that are sensitive to the long-range intramolecular interactions of even spatially remote parts of molecules and can give valuable insight into the structural and conformational features of organic compounds. A rather accurate probability distribution is obtained by treating experimental RDCs data sets with proper theoretical models. This means the conformational surface is explored leading to an equilibrium between global and local minima rather than a single defined conformer. In this work we apply such powerful methodology to probe the conformational distributions of *S*-(+)-naproxen (NAP) and *R*-(-)-flurbiprofen (FLU) (Fig. 1). Structurally, these drugs share some basic features: a propionic acid side chain, a central aryl moiety (naphthalene in NAP and fluorophenyl in FLU) and another terminal residue (methoxy group in NAP and unsubstituted phenyl in FLU). To access their conformational features we exploited here an organic solvent-based weakly ordering liquid crystal phase composed of the synthetic homopolypeptide poly- γ -benzyl-*L*-glutamate (PBLG) dissolved in a helicogenic co-solvent.⁴²⁻⁴³ In such helicogenic co-solvents, the main chain of the synthetic polypeptide adopts a rigid chiral α -helical conformation. Spontaneously, the chiral fibers orient themselves to form a macroscopic, supramolecular helicoïdal structure of directors in the mesophase, typical of that exhibited by cholesteric liquid crystals. When submitted to a routine NMR magnetic field, the supramolecular helix unwinds, and the system behaves like a chiral nematic phase with positive anisotropy of the molecular diamagnetic susceptibility, with the directors homogeneously aligned parallel to the static magnetic field. Note that the organic co-solvent employed has to homogeneously dissolve the polypeptide and preserve the α -helical structure of the polymer. Therefore, solvents that form strong hydrogen bonds with the polypeptide chain are not suitable as co-solvent since they cause the loss of liquid crystalline properties. The potential of such ordered media has been largely demonstrated in various applications as structural and relative configuration determinations,⁴⁴⁻⁴⁵ enantiomeric excesses measurements⁴⁶⁻⁵⁰ or discussion of reaction pathways involving several organic functional groups and NMR isotopes.⁵¹⁻⁵² Recently a PBLG phase was also used to investigate the conformational equilibrium of a small difluorinated drug.⁵³ In the present study the experimental RDCs measured for NAP and FLU will be interpreted by means of the robust theoretical approach known as the AP-DPD

model⁵⁴⁻⁵⁵ to obtain their conformational distribution in solution.

Results and discussion

NMR Spectral Analysis in Weakly Ordering PBLG Phase.

The magnetic interactions we are interested in are the observed RDCs, D_{ij}^{obs} , between the i -th and j -th magnetically active nuclei of the molecule. RDCs are normally averaged out to zero in isotropic media because of Brownian reorientational motion. On the contrary, they become readily observable when the solute is partially oriented in aligning media. Here we chose to use as partially ordered solvent the nowadays quite popular chiral nematic liquid crystalline phase composed of PBLG dissolved in the helicogenic organic co-solvent THF- d_8 . Contrarily to highly ordering media like thermotropic liquid crystals, a molecule dissolved in PBLG phases turns out to have a low degree of orientational order. This allows the magnitude of dipolar couplings to be comparable to or even smaller than that of scalar couplings. Consequently, the spectral quality of high-resolution mostly first-order NMR spectra is usually retained. Moreover, the use of a PBLG-organic co-solvent mixture has the additional advantage of overcoming the problem of very poor water solubility of the chosen drugs NAP and FLU.

RDCs cannot be directly extracted from the anisotropic spectra of FLU and NAP dissolved in PBLG/THF- d_8 . Indeed, they should be calculated as follows:⁵³

$$D_{ij} = \frac{\pm T_{ij}^{obs} - (\pm J_{ij}^{iso})}{2} \quad (\text{for } i \text{ and } j \text{ non - equivalent nuclei}) \quad (1)$$

or

$$D_{ij} = \frac{\pm T_{ij}^{obs}}{3} \quad (\text{for } i \text{ and } j \text{ equivalent nuclei}) \quad (2)$$

where T_{ij}^{obs} is the total coupling constant that is measured from the NMR spectra of the anisotropic samples (NAP/PBLG/THF- d_8 and FLU/PBLG/THF- d_8) and J_{ij}^{iso} is the scalar coupling that is measured from the isotropic spectra in the same organic solvent (NAP/THF- d_8 and FLU/THF- d_8).

On both the isotropic and anisotropic samples, 1D NMR ^1H , ^{13}C , $^{13}\text{C}\{-^1\text{H}\}$, $^{13}\text{C}\{-^{19}\text{F}\}$ and ^{19}F spectra were recorded. Spectral assignment of the peaks was performed on the basis of COSY, HSQC and HMBC correlation experiments. The extraction of as large as possible sets of J_{ij} and T_{ij} couplings between nuclear pairs $^1\text{H}\{-^1\text{H}\}$, $^1\text{H}\{-^{13}\text{C}\}$ and $^{19}\text{F}\{-^{13}\text{C}\}$ is not a trivial task and required both standard experiments, like 1D $^{13}\text{C}\{-^1\text{H}\}$ and 2D $^1\text{H}\{-^{13}\text{C}\}$ J -resolved spectra, and more sophisticated pulse sequences, such as 2D $^1\text{H}\{-^1\text{H}\}$ SERF,⁵⁶ $^1\text{H}\{-^{19}\text{F}\}$ HF-SERF,⁵⁷ and $^1\text{H}\{-^{13}\text{C}\}$ HETSERF⁵⁸ experiments. It is worth emphasising that, contrarily to isotropic media, in PBLG phases even dipolar couplings between the three equivalent protons of each methyl groups (H_3 and H_{14}) affect the NMR spectrum. For instance, in NAP (Fig. 2) H_3 gives a triplet of doublets due to the coupling between the three equivalent protons of the methyl group and the coupling with the proton H_2 directly attached to the stereogenic carbon atom. Albeit not well resolved in the ^1H 1D spectrum (Fig. 2a), this multiplet structure is evident in the homonuclear SERF experiment shown in Fig. 2b.

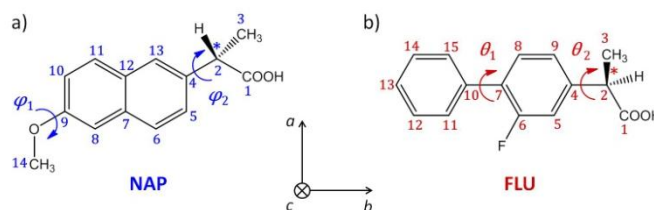


Figure 1. Topological structure, carbon atoms labelling and torsional angle $\varphi_1 = \text{C}_8\text{-C}_9\text{-O-C}_{14}$, $\varphi_2 = \text{C}_{13}\text{-C}_4\text{-C}_2\text{-H}_2$, $\theta_1 = \text{C}_8\text{-C}_7\text{-C}_{10}\text{-C}_{15}$ and $\theta_2 = \text{C}_5\text{-C}_4\text{-C}_2\text{-H}_2$ of (a) *S*-naproxen (NAP) and (b) *R*-flurbiprofen (FLU). Protons and fluorine nuclei are numbered after the carbon they are bound to. The (a, b, c) axes of the molecular reference frame adopted for the molecules are also shown.

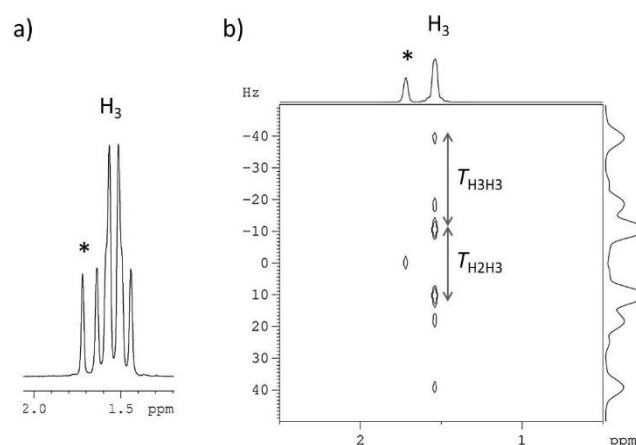


Figure 2. (a) Signal corresponding to H_3 extracted from the 1D ^1H spectrum (Larmor frequency 400.13 MHz) recorded on *S*-naproxen in PBLG/THF- d_8 at 300 K. (b) 2D $^1\text{H}\{-^1\text{H}\}$ SERF tilted spectrum (Larmor frequency 400.13 MHz) of the same sample where the offset of the excitation selective pulse was set at ν_3 and the offsets of the refocalisation selective pulse at ν_2 and at ν_3 . This experiment let the H_3H_3 and H_2H_3 couplings evolve in t_1 so they can be trivially measured on the F_1 dimension. The SERF spectrum was recorded in 26 min using a data matrix of 2048 (t_2) \times 64 (t_1) with 16 scans per t_1 increment. The relaxation delays were 1 s. Data were processed using zero-filling up to 256 points and a sine filter in both dimensions. The duration of the RE-BURP refocusing and the E-BURP excitation pulses was 12.4 ms, corresponding to a frequency width of 400 Hz. Solvent peaks are labeled with asterisks.

For the measurement of the $^1\text{H}\{-^{13}\text{C}\}$ long range couplings, especially those between spins belonging to different fragments of the molecule (*i.e.* methoxy group, naphthalene and propionic fragment for NAP, unsubstituted ring, fluorinated ring and propionic fragment for FLU), we applied the heteronuclear selective refocusing $^{13}\text{C}\{-^1\text{H}\}$ NMR experiment, HETSERF, originally developed for the measurement of long-range $^1\text{H}\{-^{13}\text{C}\}$ scalar couplings in isotropic media,⁵⁸ and then applied to the extraction of short- and long-range total spin-spin couplings in solutes dissolved in chiral liquid crystals.⁵⁹ This pulse sequence proved to be a valuable help for editing critical dipolar couplings between aromatic carbons and aliphatic protons. As an example, Fig. 3b displays the HETSERF spectrum recorded on FLU/PBLG/THF- d_8 selecting H_2 on the proton channel. It can be observed that the heteronuclear selective spectrum allows total couplings such as $^2T_{\text{C}_4\text{H}_2}$, $^3T_{\text{C}_5\text{H}_2}$, and $^3T_{\text{C}_9\text{H}_2}$,

which cannot be measured in the proton-coupled ^{13}C 1D spectrum (Fig. 3a), to be easily edited.

Some more spectra are reported in Figures 1-11 of ESI. From all the experiments large sets of J_{ij} and T_{ij} were measured, which are reported together with the chemical shifts in Tables 1-3 of ESI. The sets of desired D_{ij}^{obs} were calculated from the totality of experimental J_{ij} and T_{ij} couplings, following an already applied strategy,^{53,60-61} for a total of 34 independent D_{ij}^{obs} for NAP and 39 for FLU (reported in Tables 1 and 2, respectively). Note that, for both molecules, no dipolar coupling between the proton of carboxyl group and the other nuclei of the molecule has been extracted. Hence the lack of these experimental data did not enable us to investigate the possible different orientations of the carboxyl group.

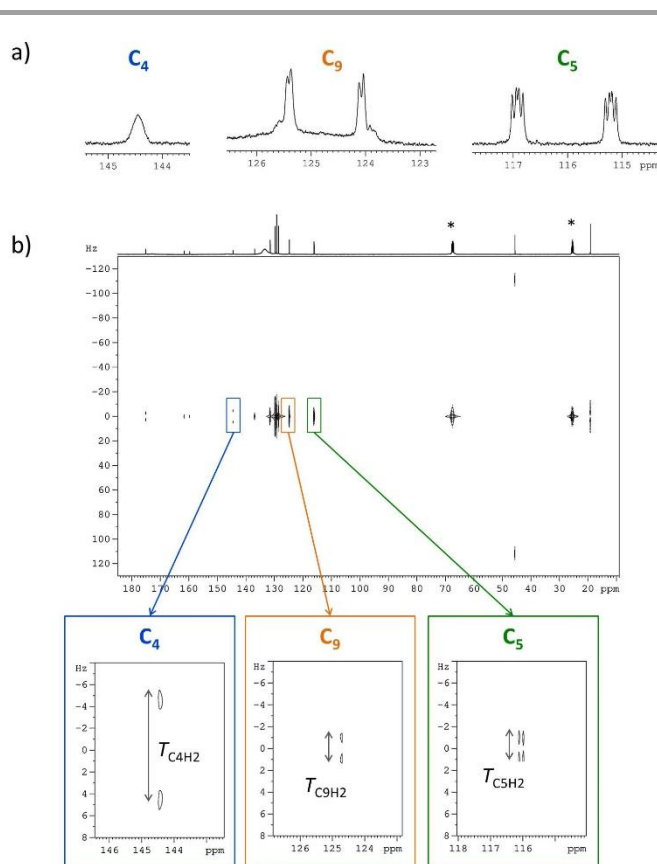


Figure 3. (a) Signals of some selected aromatic carbons (C_4 , C_9 and C_5) extracted from the 1D proton-coupled ^{13}C spectrum (Larmor frequency 125.76 MHz) of *R*-flurbiprofen in PBLG/THF- d_8 . The spectrum was recorded at 304 K by using 65536 points and 14336 scans and processed using an exponential filter (LB = 0.8 Hz). (b) 2D ^{13}C - ^1H HETSERF spectrum (^1H and ^{13}C Larmor frequencies 500.13 and 125.76 MHz, respectively) of the same sample where the offset of the π selective pulse on the proton channel was set at u_2 . The HETSERF spectrum was recorded in 9 h using a data matrix of 4096 (t_2) \times 200 (t_1) with 80 scans per t_1 increment. The relaxation delays were 1.5 s. Data were processed using zero-filling on t_1 up to 512 points and no filter. The duration of the RE-BURP refocusing pulse was 12.4 ms corresponding to a frequency width of 400 Hz. Enlarged maps of selected carbon signals (C_4 , C_9 and C_5) are also shown. Solvent peaks are labeled with asterisks.

Table 1. Experimental dipolar couplings D_{ij}^{obs} determined by the NMR analysis of NAP dissolved in PBLG/THF, compared with the D_{ij}^{calc} values. Good agreement implies a small RMS value.

i	j	D_{ij}^{obs} [a] (Hz)	D_{ij}^{calc} [b] (Hz)
C-H couplings			
C_2	H_2	58.3 ± 0.6	58.3
C_2	H_5	1.6 ± 0.5	1.4
C_3	H_2	5.6 ± 0.5	5.3
C_3	H_3	-6.4 ± 0.6	-6.6
C_4	H_2	-1.3 ± 0.6	-2.0
C_4	H_3	-0.1 ± 0.6	-0.4
C_4	H_5	7.4 ± 0.6	6.9
C_5	H_2	-1.1 ± 0.6	-1.1
C_5	H_5	7.2 ± 0.7	7.3
C_5	H_{13}	1.7 ± 0.5	1.8
C_6	H_6	40.2 ± 0.6	39.5
C_7	H_5	-0.9 ± 0.7	-1.2
C_8	H_8	37.6 ± 0.6	37.8
C_8	H_{11}	0.7 ± 0.6	0.8
C_8	H_{14}	-2.2 ± 0.7	-2.4
C_{10}	H_8	1.9 ± 0.6	1.8
C_{10}	H_{10}	8.0 ± 0.6	7.9
C_{11}	H_8	0.8 ± 0.6	0.8
C_{11}	H_{11}	37.5 ± 0.7	38.2
C_{11}	H_{13}	-4.8 ± 0.6	-4.5
C_{13}	H_2	-3.0 ± 0.7	-3.5
C_{13}	H_5	1.5 ± 0.7	1.5
C_{13}	H_{13}	38.0 ± 0.8	38.5
C_{14}	H_8	-3.4 ± 0.6	-3.7
C_{14}	H_{14}	-5.4 ± 0.6	-5.2
H-H couplings			
H_2	H_3	6.7 ± 0.5	6.5
H_2	H_5	-3.4 ± 0.2	-3.2
H_3	H_3	-9.7 ± 0.5	-9.8
H_3	H_5	0.5 ± 0.2	0.4
H_5	H_6	-22.1 ± 0.3	-22.6
H_5	H_8	-3.1 ± 0.3	-3.1
H_5	H_{14}	-1.0 ± 0.2	-0.8
H_6	H_8	-17.6 ± 0.3	-17.2
H_6	H_{10}	0.9 ± 0.3	0.6
H_6	H_{11}	2.2 ± 0.3	1.6
H_6	H_{13}	1.7 ± 0.3	1.6
H_6	H_{14}	-2.1 ± 0.2	-2.1
H_8	H_{10}	3.5 ± 0.3	3.4
H_8	H_{11}	1.8 ± 0.3	1.6
H_8	H_{14}	-14.6 ± 0.3	-14.8
H_{10}	H_{11}	-24.4 ± 0.3	-23.8
H_{11}	H_{13}	-16.7 ± 0.3	-17.4
H_{14}	H_{14}	-7.3 ± 0.3	-7.4
RMS [c]		0.40 Hz	

[a] calculated from eqs. (1) and (2)

[b] from the AP-DPD method

[c] $\text{RMS} = \left\{ M^{-1} \sum_{i < j} [D_{ij}^{obs} - D_{ij}^{calc}]^2 \right\}^{\frac{1}{2}}$ (M = number of independent couplings)

Molecular Modelling Calculations.

Aiming at determining the conformational distribution of the two profens, the *a priori* knowledge of the geometry of the most stable conformers and a good estimate of the potential energy surface

(PES) is required. Hence, a molecular dynamics calculation was first performed by the MD module of HyperChemTM software package,⁶² refining the geometries with the semi-empirical AM1 method, in order to individuate approximately structures and locations of the lowest minimum energy conformers *in vacuo*. An accurate geometry optimization was performed then on the minimum energy structures at DFT level by means of the B3LYP hybrid density functional with the basis set 6-31++G**, using the Gaussian03 software package.⁶³ The same results were obtained by directed or Monte-Carlo (Metropolis algorithm) conformational search instead of MD simulations.⁶² Theoretical calculations predicted four minimum energy conformers for NAP (Table 3) and four couples of symmetry-related conformers for FLU, as expected from the symmetry of the unsubstituted ring (Table 4).

In the molecule of *S*-naproxen, the O-C₁₄ bond lies preferentially in the plane of the aromatic ring. The conformers I and II, where the methoxy group adopts a *cis* orientation with respect to the C₈-C₉ aromatic bond ($\varphi_1 \sim 0^\circ$), are about 6 kJ/mol more stable than their *trans* analogues III and IV. The theoretical Boltzmann distribution of the four conformers can be roughly calculated from the potential energy values as:

$$P_{theo}(\varphi) \propto \exp(-E_{pot}^{rel}/RT) \quad (3)$$

where T denotes the absolute temperature and R the universal gas constant. From eq. (3) we obtained that isomers I and II count for more than 90% with respect to conformers III and IV. The conformational preference for the *cis* configuration of the methoxy group has already been found for naproxen and analogues.^{18,64-67}

The main difference in the geometry of the conformers is in the value of the C₈-C₉-O angle: for the conformers I and II this angle is approximately 126° while for the conformers III and IV is about 116°.

For the molecule of *R*-flurbiprofen, the torsion angle θ_1 between the two rings is about $\pm 43^\circ$ and $180^\circ \pm 43^\circ$, in agreement with previous calculations *in vacuo* and in water solution,⁶⁸ and about 10° smaller than the torsion angle found experimentally and theoretically in the crystalline structure.⁶⁹

As for the torsion angles of the chiral substituent around the C₂-C₄ axis, φ_2 and θ_2 , the theoretical values indicate that both in NAP and FLU the two bulky methyl and carboxylic acid groups are located on each side of aromatic plane (naphthalene or fluorinated ring) to minimize steric repulsion, while the hydrogen atom directly bound to the stereogenic carbon atom (α -hydrogen) lies almost in the aromatic plane. This *quasi*-planarity of the α -hydrogen atom relative to the aromatic ring is indeed a common feature of arylacetates, as widely observed in the literature.^{13,64,68} Moreover, conformations with the α -hydrogen opposite to the other substituent of the aromatic system (-OCH₃ or -F) turn out to be slightly stabilized, with relative percentages of about 60%.

In order to further verify the results and not to skip local minima, relaxed PES scans (*i.e.* allowing for bond lengths and angles relaxation of the structure) were performed separately (assuming the independence of the two rotations) for the torsion angles φ_1 and φ_2 in NAP and θ_1 and θ_2 in FLU. Results confirmed the previous observations and are reported in Figures 12 and 13 of ESI.

Note finally that no significant difference in terms of structure and relative energies of the most stable conformers emerged by

changing the functional and the basis set from B3LYP/6-31++G** to MP2/6-31G.

Table 2. Experimental dipolar couplings D_{ij}^{obs} determined by the NMR analysis of FLU dissolved in PBLG/THF, compared with the D_{ij}^{calc} values. Good agreement implies a small RMS value.

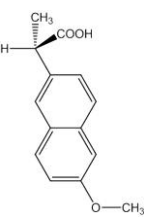
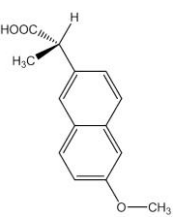
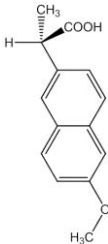
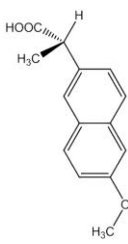
<i>i</i>	<i>j</i>	D_{ij}^{obs} [a] (Hz)	D_{ij}^{calc} [b] (Hz)
<i>C-H couplings</i>			
C ₁	H ₂	1.2 ± 0.5	2.1
C ₁	H ₃	1.3 ± 0.5	1.0
C ₁	H ₅	-1.0 ± 0.6	-1.0
C ₂	H ₂	46.3 ± 0.3	46.4
C ₂	H ₃	2.1 ± 0.5	2.2
C ₃	H ₂	5.3 ± 0.6	5.2
C ₃	H ₃	-8.3 ± 0.3	-8.6
C ₄	H ₂	-1.3 ± 0.6	-2.1
C ₄	H ₃	0.0 ± 0.6	-0.3
C ₅	H ₂	-1.7 ± 0.6	-2.2
C ₅	H ₃	0.0 ± 0.5	-0.6
C ₅	H ₅	27.3 ± 0.3	27.7
C ₅	H ₉	1.1 ± 0.3	1.1
C ₈	H ₈	24.6 ± 0.6	24.1
C ₉	H ₂	-1.7 ± 0.5	-1.8
C ₉	H ₃	0.0 ± 0.5	-0.5
C ₉	H ₈	-4.5 ± 0.3	-4.3
C ₉	H ₉	4.8 ± 0.3	4.9
C ₁₁	H ₁₁	23.5 ± 0.6	23.8
C ₁₅	H ₁₅	23.5 ± 0.6	23.8
C ₁₂	H ₁₁	-5.5 ± 0.4	-5.0
C ₁₄	H ₁₅	-5.5 ± 0.4	-5.0
C ₁₂	H ₁₂	23.9 ± 0.6	23.7
C ₁₄	H ₁₄	23.9 ± 0.6	23.7
C ₁₃	H ₁₃	-60.8 ± 0.6	-60.4
<i>H-H couplings</i>			
H ₂	H ₃	7.5 ± 0.3	7.4
H ₂	H ₅	-9.7 ± 0.2	-10.1
H ₂	H ₈	-1.5 ± 0.2	-1.4
H ₂	H ₉	-5.7 ± 0.2	-5.7
H ₃	H ₃	-12.3 ± 0.1	-12.3
H ₃	H ₅	-3.0 ± 0.2	-3.0
<i>H-F couplings</i>			
H ₅	F ₆	-18.0 ± 0.2	-18.3
H ₈	F ₆	2.0 ± 0.2	2.0
H ₁₁	F ₆	-3.1 ± 0.2	-3.0
H ₁₅	F ₆	-3.1 ± 0.2	-3.0
<i>C-F couplings</i>			
C ₂	F ₆	-0.7 ± 0.3	-0.5
C ₄	F ₆	-0.7 ± 0.3	-0.7
C ₅	F ₆	-4.1 ± 0.3	-4.1
C ₆	F ₆	4.0 ± 0.3	4.0
C ₇	F ₆	3.6 ± 0.3	3.4
C ₈	F ₆	0.9 ± 0.3	0.8
C ₉	F ₆	0.1 ± 0.3	0.1
C ₁₁	F ₆	-0.3 ± 0.3	-0.3
C ₁₅	F ₆	-0.3 ± 0.3	-0.3
RMS [c]		0.34 Hz	

[a] calculated from eqs. (1) and (2)

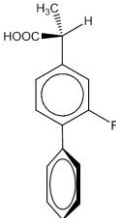
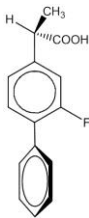
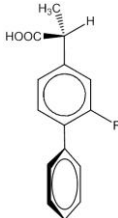
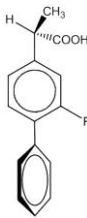
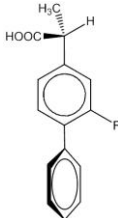
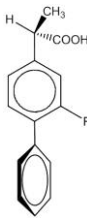
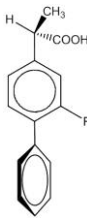
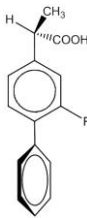
[b] from the AP-DPD method

[c] $RMS = \left\{ M^{-1} \sum_{i < j} [D_{ij}^{obs} - D_{ij}^{calc}]^2 \right\}^{\frac{1}{2}}$ (M = number of independent couplings)

Table 3. Relative energies and probabilities, sketched structures and selected dihedral angles of the four lowest minimum energy conformers obtained for NAP from B3LYP/6-31++G** calculations.

Conformers	I	II	III	IV
				
E_{pot}^{rel} (kJ/mol)	0.00 ^[a]	1.18	6.31	7.25
$\varphi_1 = C_8-C_9-O-C_{14}$ (degree)	0.48	0.05	179.97	180.02
$\varphi_2 = C_{13}-C_4-C_2-H_2$ (degree)	5.61	186.71	5.13	186.07
$C_{13}-C_4-C_2-C_3$ (degree)	244.88	66.01	244.37	65.32
$C_{13}-C_4-C_2-C_1$ (degree)	121.42	302.44	120.89	301.75
P_{theo} (%) ^[b]	56.9	35.4	4.6	3.1

^[a] arbitrarily fixed at 0 kJ/mol^[b] calculated from eq. (3)**Table 4.** Relative energies and probabilities, sketched structures and selected dihedral angles of the four pairs of lowest minimum energy conformers obtained for FLU from B3LYP/6-31++G** calculations.

Conformers	I	I*	II	II*	III	III*	IV	IV*
								
E_{pot}^{rel} (kJ/mol)	0.73	0.73	0.00 ^[a]	0.00	0.89	0.89	0.17	0.17
$\theta_1 = C_8-C_7-C_{10}-C_{15}$ (degree)	42.63	223.91	42.32	223.66	136.17	317.47	135.46	316.74
$C_6-C_7-C_{10}-C_{11}$ (degree)	44.52	223.27	44.42	222.91	136.76	315.49	135.96	314.87
$\theta_2 = C_5-C_4-C_2-H_2$ (degree)	0.83	0.82	179.92	179.98	0.60	0.69	180.12	180.55
$C_5-C_4-C_2-C_3$ (degree)	121.02	121.00	300.04	300.09	120.78	120.88	300.22	300.68
$C_5-C_4-C_2-C_1$ (degree)	247.68	247.67	66.68	66.75	247.43	247.52	66.84	67.29
P_{theo} (%) ^[b]	11.0	11.0	14.8	14.8	10.3	10.3	13.8	13.8

^[a] arbitrarily fixed at 0 kJ/mol^[b] calculated from eq. (3)

Strategy for the Conformational Analysis.

The observed RDCs that have been extracted from the NMR analysis of the two flexible molecules NAP and FLU dissolved in the PBLG/THF- d_8 liquid-crystalline phase, having positive diamagnetic anisotropy, result from the average over all the ϕ conformations and can be approximated to:^{53,70}

$$D_{ij}^{obs} \approx \frac{2}{3} \cdot \frac{Z_{iso}}{Z} \cdot \int P_{iso}(\{\phi\}) Z_{ext}(\{\phi\}) \sum_{\alpha\beta} S_{\alpha\beta}(\{\phi\}) D_{ij,\alpha\beta}(\{\phi\}) d\{\phi\} \quad (4)$$

where $\{\phi\}$ is the set of internal angles defining the conformation and Z , Z_{iso} and $Z_{ext}(\{\phi\})$ are proper normalization factors. The term $P_{iso}(\{\phi\})$ is the pertinent conformational target: it defines the probability distribution of the solute in a conventional isotropic liquid sharing, at the experimental temperature, the same physical properties of the liquid-crystalline solvent, except for its ability to

induce a solute ordering. The terms $S_{\alpha\beta}(\{\phi\})$ are the solute orientational order parameters, constituting the real symmetric traceless Saupe ordering matrix, and the $D_{ij,\alpha\beta}(\{\phi\})$ are the Cartesian components, given in the molecular frame, of the D_{ij} dipolar coupling tensor between the i -th and the j -th nucleus. The main consequence of eq. (4) is that, in order to extract the desired conformational information from the experimental D_{ij}^{obs} , it is necessary to adopt a theoretical model describing both the conformation-orientation anisotropic interactions and $P_{iso}(\{\phi\})$. Here we used the so-called AP-DPD approach, that is a combination of the Additive Potential model,⁵⁴ for the treatment of the ordering interactions, with the Direct Probability Description⁵⁵ of the torsional distribution $P_{iso}(\{\phi\})$ (for a rigorous theoretical description the reader is referred to refs 36 and 70). Within the AP model, the orientational interaction energy is described by a spherical harmonics expansion whose $\{\phi\}$ -dependent coefficients can be conveniently constructed as a sum of $\{\phi\}$ -independent

tensorial contributions $\varepsilon_{2,p}^j$ from each rigid fragment j of the molecule. In practice, the $\varepsilon_{2,p}^j$ are unknown quantities whose values are adjusted to obtain the best agreement with the experimental data. Concerning the DPD approach, its strength is that the $P_{iso}(\{\phi\})$ can be modeled in terms of Gaussian functions. NAP and FLU are two-rotor molecules. Indeed, two flexible substituents (methoxy group/unsubstituted ring and propionic fragment) may take different orientations with respect to the central aromatic system (naphthalene and fluorinated ring) by rotation around the dihedral angles φ_1, φ_2 for NAP and θ_1, θ_2 for FLU, and lead to several stable isomers (Fig. 1). Therefore, the torsional distribution $P_{iso}(\{\phi\})$ corresponds to $P_{iso}(\varphi_1, \varphi_2)$ and $P_{iso}(\theta_1, \theta_2)$, respectively.

From the operative point of view, the conformational analysis is performed by the AP-DPD theoretical approach, through a dedicated software called AnCon,⁷¹ starting from the experimental RDCs. The geometry of the rigid subunits is fixed as from molecular modelling calculations (Tables 4 and 5 of ESI). In the procedure a set of calculated dipolar couplings D_{ij}^{calc} (obtained by a trial set of orientational, geometrical and conformational parameters) is fitted against the experimental one, while iterating on a pertinent number of unknowns, till their optimised values. Such unknowns include the orientational parameters, *i.e.* the set of chosen $\varepsilon_{2,p}^j$ solute-solvent interaction tensor elements, and the conformational parameters, *i.e.* the terms needed to model the conformational probability in terms of Gaussian functions. During the iterative process, the unknown parameters are adjusted in order to reproduce the whole set of D_{ij}^{obs} , until an acceptable value for the RMS (root mean square) function, evaluated on the differences between the experimental and calculated dipolar couplings, is reached.

As previously assumed, the torsional distributions for the two dihedral angles are non-cooperative motions, due to the limited interactions between the fragments. Therefore, the more convenient strategy to describe the conformational distribution for these protons is a two-step approach:

- 1) each non-cooperative motion is first treated separately, in order to quickly optimise the orientational and conformational parameters, avoiding huge computational burden;
- 2) the two non-cooperative rotations are combined together as a simple product, in order to describe the conformational surface for the whole molecule.

Conformational distribution of S-Naproxen.

Torsional distribution for the 2-methoxynaphthalene fragment. To describe the torsional distribution around φ_1 , involving the rotation of the methoxy group, M , with respect to the naphthalene, N , we considered the fragment 2-methoxynaphthalene. Within the AP model, this portion of the molecule can be described by 4 fragment tensors: $\varepsilon_{C_6,C_{13}}$ and ε_{C_5,C_7} for the biaxial fragment N ; $\varepsilon_{C_9,O}$ and $\varepsilon_{O,C_{14}}$ for the monoaxial components along the respective bond directions. Within the DPD model the torsional probability distribution around φ_1 , $P_{iso}(\varphi_1)$, has been modelled as a balanced sum of two Gaussian functions centred at 0° and 180° that can be written as follows:

$$P_{iso}(\varphi_1) = \left(\frac{|\cos\varphi_1| - \cos\varphi_1}{2} + A_{\varphi_1} \cos\varphi_1 \right) \cdot \exp \left[-\frac{\sin^2(\varphi_1 - \varphi_1^{max})}{2h_{\varphi_1}^2} \right] \quad (5)$$

where φ_1^{max} is the first most probable value of the torsion angle (the second one being $180^\circ + \varphi_1^{max}$), A_{φ_1} is the relative weight of the first Gaussian (the relative weight of the second Gaussian is fixed to be equal to $1 - A_{\varphi_1}$) and, finally, h_{φ_1} gives the width at half maximum height of each Gaussian.

Fixing the geometry of the molecular subunits as from molecular modelling calculations, a subset of 23 independent D_{ij}^{obs} of Table 1 corresponding to the 2-methoxynaphthalene portion of the molecule (16 for N , 2 for M and 5 between the two fragments) was fitted, while iterating on 5 unknowns, namely the 4 orientational parameters and, separately, on the conformational terms φ_1^{max} and A_{φ_1} , and parametrically adjusting h_{φ_1} , until an acceptable value for the RMS target function is reached. Note that for the C_8-C_9-O angle an averaged value weighed on the individual theoretical conformers has been used as shown in Table 4 of ESI. After optimization we obtained the torsional distribution $P_{iso}(\varphi_1)$ reported in Figure 4a (blue solid line), which is characterized by an absolute maximum at 0° with relative percentage of 87% and a relative maximum at 180° with relative percentage of 13%. The C_9-O-C_{14} plane is then arranged almost coplanar with the naphthalene with a preference for the *cis* configuration of the methoxy group relative to the C_8-C_9 bond. The result is in agreement with the theoretical probability distribution, $P_{theo}(\varphi_1)$ (blue dashed line), calculated from the potential energy values obtained by DFT calculations, with only a slight change in the probability ratio between the two conformers (90:10 in $P_{theo}(\varphi_1)$ versus 87:13 in experimental $P_{iso}(\varphi_1)$).

Torsional distribution for the S-(+)-2-(2-naphthyl)propionic acid fragment. The dihedral angle φ_2 describes the rotation of the propionic acid moiety, P , with respect to the naphthalene, N . For describing through the AP model this fragment, 6 tensor elements are required: $\varepsilon_{C_6,C_{13}}$ and ε_{C_5,C_7} for N ; ε_{C_4,C_2} , ε_{C_2,H_2} , ε_{C_2,C_3} and ε_{H_2,C_3} for the corresponding monoaxial components. As for the DPD model, the same expression used previously for $P_{iso}(\varphi_1)$ works well for the rotation of the propionic fragment, since the two lowest energy conformers derive from a rotation of about 180° of the whole chiral substituent around the C_2-C_4 bond. Then to describe $P_{iso}(\varphi_2)$ we have to optimise the conformational terms φ_2^{max} , A_{φ_2} and h_{φ_2} . As previously done, calculations were performed by fixing molecular geometry as from DFT calculations and by varying φ_2^{max} and A_{φ_2} separately, with a parametrical adjustment of h_{φ_2} . The set of 7 unknowns was adjusted while fitting the subset of 27 independent D_{ij}^{obs} (16 for N , 7 for P and 4 between the two fragments) of Table 1 corresponding to the naphthylpropionic acid moiety of the molecule. The torsional distribution $P_{iso}(\varphi_2)$ obtained after optimization is reported in Figure 4b (pink solid line), together with the theoretical probability distribution, $P_{theo}(\varphi_2)$ (pink dashed line) calculated from the potential energy values obtained by DFT calculations. Experimental $P_{iso}(\varphi_2)$ displays an absolute maximum at 16° with relative percentage of 66% and a relative maximum at 196° with relative percentage of 34%. As before, the experimental curve is similar to the theoretical one, indicating the *quasi*-planarity of the α -

hydrogen atom relative to the aromatic ring with a slight preference for the *cis* configuration relative to the C₄-C₁₃ bond. Even though the φ_2^{max} value is affected by a considerable error, a small but not negligible shift from about 6° in DFT calculations to 16°±6° in the AP-DPD conformational analysis can be observed.

Torsional distribution for the whole molecule. Since the propanoic and the methoxy groups are relatively far from each other in the molecular structure, it can be safely assumed that the rotations around the two dihedral angles φ_1 and φ_2 are non-cooperative motions. Hence, the total probability distribution function $P_{iso}(\varphi_1, \varphi_2)$ describing the whole molecular conformational surface is simply the renormalized product between the single probability distributions for each torsion:

$$P_{iso}(\varphi_1, \varphi_2) = P_{iso}(\varphi_1) \cdot P_{iso}(\varphi_2) \quad (6)$$

For the definition of the fragment tensors $\varepsilon_{2,p}^j$ for the whole molecule, we just need to add the interaction tensors defined for the two substructures considered before. A simplification is obtained considering that the direction of the C₉-O and C₄-C₂ bonds is parallel, thus $\varepsilon_{C_9,O} = \varepsilon_{C_4,C_2}$. Definitely, 7 $\varepsilon_{2,p}^j$ are required: $\varepsilon_{C_6,C_{13}}$ and ε_{C_5,C_7} for the *N* fragment; $\varepsilon_{O,C_{14}}$ for the *M* fragment; ε_{C_2,H_2} , ε_{C_2,C_3} and ε_{H_2,C_3} for the *P* fragment; $\varepsilon_{C_9,O} = \varepsilon_{C_4,C_2}$ for connecting *N*, *P* and *M*. The whole set of 34 independent D_{ij}^{obs} of Table 1 was fitted while iterating on 7 orientational parameters, fixing the six conformational terms (φ_1^{max} , φ_2^{max} , A_{φ_1} , A_{φ_2} , h_{φ_1} and h_{φ_2}) at the optimised values found for the single rotations. A satisfactory RMS error of 0.40 was reached, with a good reproduction of D_{ij}^{obs} (see Table 1), as it can be seen in Figure 5a.

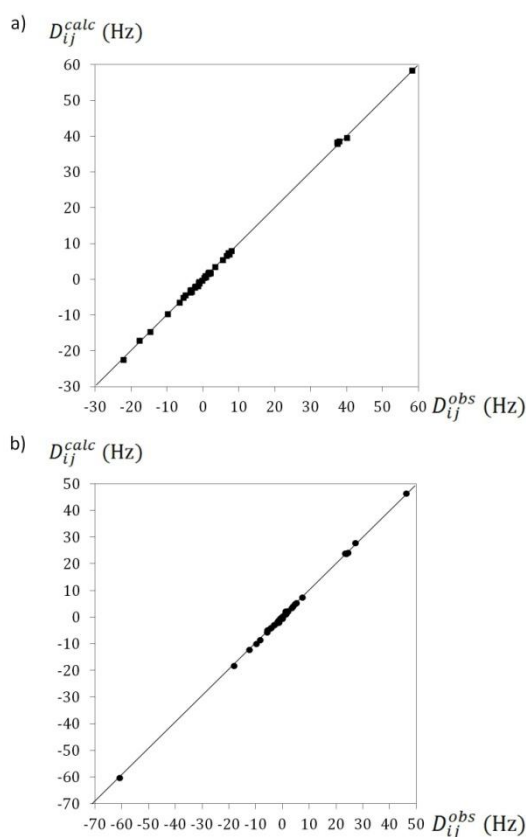


Figure 5. Observed versus theoretical dipolar couplings obtained for (a) NAP and (b) FLU from NMR experiments and by the AP-DPD approach, respectively.

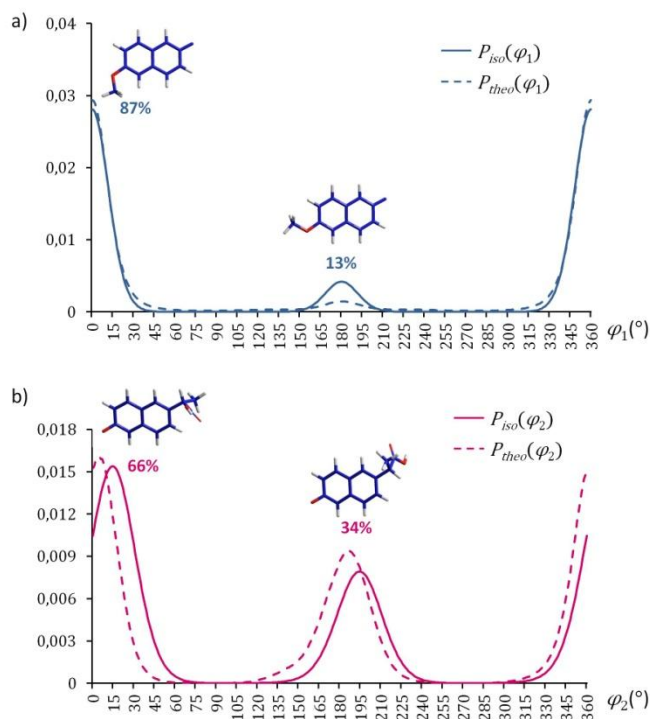


Figure 4. Experimental (solid line) and theoretical (dashed line) torsional probability distributions as a function of (a) φ_1 and (b) φ_2 , obtained for *S*-naproxen respectively by the AP-DPD approach and from B3LYP/6-31G** calculations. All curves are obtained by varying φ_1 and φ_2 over the 0° - 360° range with a 1°-step sampling.

The optimised parameters are reported in Table 6 of ESI. The experimental torsional distribution $P_{iso}(\varphi_1, \varphi_2)$ (Fig. 6) is characterized by four more populated structures. Conformers I and II, having $\varphi_1 \sim 0^\circ$ and φ_2 respectively equal to $\sim 16^\circ$ and $\sim 196^\circ$, are the most stable conformers, with relative percentages of 57.4% and 29.6%. The isomers III and IV involving the *trans* geometry of the methoxy group ($\varphi_1 \sim 180^\circ$) and the same geometry of the chiral side chain (φ_2 equal to $\sim 16^\circ$ and $\sim 196^\circ$, respectively) are less stable than their *cis* analogues, showing relative percentages of 8.6% and 4.4%.

To stress the obtained conformational result note that a previous attempt to experimentally refine the spatial arrangement of NAP in solution was done by 2D ¹H nOe measurements.⁶⁵ For the methoxy group results indicated that a single conformation at $\varphi_1 \sim 0^\circ$ can be assumed to be almost exclusively populated. However, the description of the torsion around the C₂-C₄ axis turned out to be more complex: although nOe data were better reproduced taking into account an average of more theoretical conformations with respect to a mono-conformational model, it was not possible to unambiguously distinguish between the different bi- or tri-conformational models.

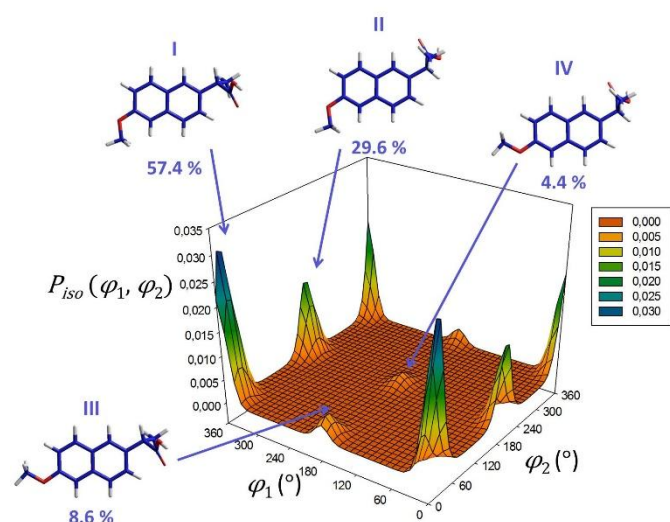


Figure 6. Experimental probability distribution $P_{iso}(\varphi_1, \varphi_2)$ obtained by AP-DPD approach for *S*-naproxen dissolved in PBLG/THF-*d*₈, including structures of minimum energy conformers and their relative abundance. The surface is obtained by varying φ_1 and φ_2 over the 0° - 360° range with a 10°-step sampling.

Conformational distribution of *R*-Flurbiprofen.

Torsional distribution for 2-fluoro-1,1'-biphenyl fragment. From a chemical point of view, FLU belongs to biphenyl homologues series, with θ_1 the torsion angle between the unsubstituted ring (*rH*) and the fluorinated ring (*rF*). Within the AP model the 2-fluoro-1,1'-biphenyl moiety is described by using 5 fragment tensors: ε_{C_4,C_7} and ε_{C_6,C_8} for *rF*; $\varepsilon_{C_{10},C_{13}}$ and $\varepsilon_{C_{11},C_{15}}$ for *rH*; ε_{C_6,F_6} for the corresponding monoaxial component.

As previously done for phenylsalicylic acid,⁵³ the $P_{iso}(\theta_1)$ has been modelled as a sum of four equally weighted Gaussian functions:

$$P_{iso}(\theta_1) \propto \left\{ \exp \left[-\frac{(\theta_1 - \theta_1^{max})^2}{2h_{\theta_1}^2} \right] + \exp \left[-\frac{(\theta_1 - \pi + \theta_1^{max})^2}{2h_{\theta_1}^2} \right] + \exp \left[-\frac{(\theta_1 - \frac{\pi}{2} + \theta_1^{max})^2}{2h_{\theta_1}^2} \right] + \exp \left[-\frac{(\theta_1 - \frac{\pi}{2} - \theta_1^{max})^2}{2h_{\theta_1}^2} \right] \right\} \quad (7)$$

where $\pm \theta_1^{max}$ and $180^\circ \pm \theta_1^{max}$ are the most probable values of the torsion angle and h_{θ_1} gives the width at half maximum height of each Gaussian.

Fixing the molecular geometry as from DFT calculations, a subset of 20 independent D_{ij}^{obs} of Table 2 (14 for *rF*, 4 for *rH* and 2 between the two rings) was fitted, while iterating on 6 unknowns (5 orientational terms and, separately, on the θ_1^{max} and h_{θ_1} conformational parameters), until an acceptable value for the RMS function is reached. Calculations gave the torsional distribution $P_{iso}(\theta_1)$ reported in Figure 7a (purple solid line), characterized by four equally probable conformers having $\theta_1^{max} = \pm 43.9^\circ$ and $180^\circ \pm 43.9^\circ$. This result is evidently in agreement with the optimised values obtained for an isolated molecule by the DFT calculations (purple dashed line). Note that this value of θ_1^{max} is slightly greater than the torsion angle found *via* the AP-DPD approach for biphenyl systems in ordered media with no substituents in the *ortho* position (e.g. biphenyl^{70,72} or phenylsalicylic acid⁵³). It is, instead, quite

similar to the angle found for other *ortho*-fluorinated biphenyl systems⁶¹ and for the drug diflunisal, which displays two fluorine nuclei on one ring, in the *ortho* and *para* position to the inter-ring bond.⁵³ The outcome can be reasonably associated to the steric effect that the fluorine atom in the *ortho* position has on the rotation,⁷³ while the one in the *para* position gives no hindrance to the free rotation. The presence of the fluorine atom forces the rotation of the two planes of the rings also in the crystal structure, where the torsion angle was found of -54.4° by X-ray studies.⁶⁹

Torsional distribution for the *R*-(-)-2-(3-fluorophenyl)propanoic acid fragment. To describe the torsional distribution around θ_2 we defined the fluorophenylpropanoic acid fragment (composed of the propanoic acid moiety, *P*, and the fluorinated ring *rF*) through 6 fragment tensors: ε_{C_4,C_7} , ε_{C_6,C_8} , ε_{C_6,F_6} , ε_{C_2,H_2} , ε_{C_2,C_3} and ε_{H_2,C_3} . The propionic side chain is a structural common feature for NAP and FLU (and for profens in general). Then, $P_{iso}(\theta_2)$ has the same expression as $P_{iso}(\varphi_2)$, characterised by 3 conformational terms, θ_2^{max} , A_{θ_2} and h_{θ_2} . Fixing geometry as from molecular modelling calculations, the whole set of 9 unknowns was adjusted while fitting the subset of 33 independent D_{ij}^{obs} (14 for *rF*, 10 for *P* and 9 between the two fragments) of Table 2 corresponding to the fluorophenylpropanoic acid moiety of the molecule. The number and the magnitude of the D_{ij}^{obs} made it possible to simultaneously iterate on θ_2^{max} , A_{θ_2} and h_{θ_2} , obtaining the $P_{iso}(\theta_2)$ reported in Figure 7b (orange solid line), together with the theoretical probability distribution, $P_{theo}(\theta_2)$ (orange dashed line) calculated from the potential energy values obtained by DFT calculations.

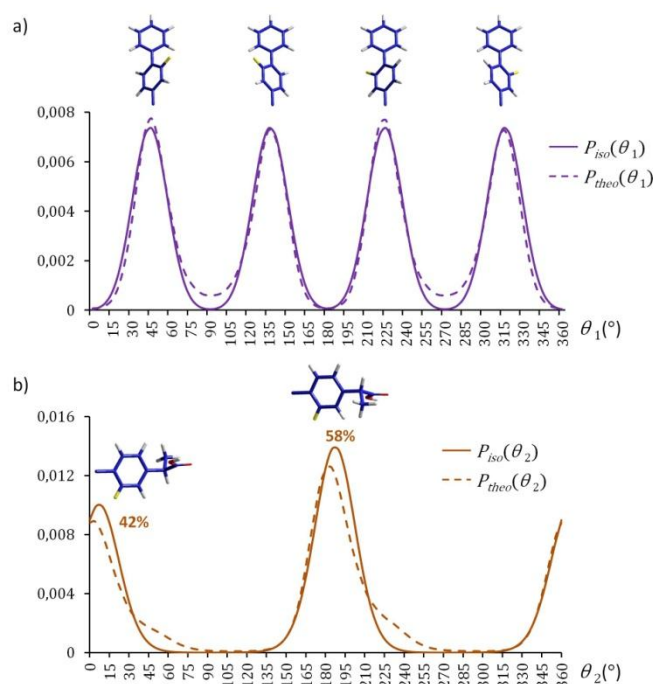


Figure 7. Experimental (solid line) and theoretical (dashed line) torsional probability distributions as a function of (a) θ_1 and (b) θ_2 , obtained for *R*-flurbiprofen respectively by the AP-DPD approach and from B3LYP/6-31G** calculations. Both curves are obtained by varying θ_1 and θ_2 over the 0° - 360° range with a 5°-step sampling.

Experimental $P_{iso}(\theta_2)$ is characterized by an absolute maximum with $\theta_2 = 187.8^\circ$ and relative percentage of 58% and a relative maximum with $\theta_2 = 7.8^\circ$ and relative percentage of 42%. As found in NAP, even considering the error affecting the θ_2^{max} value ($\sim 2^\circ$), the torsion angle found from the best fitting of the experimental RDCs is shifted towards larger values with respect to *in vacuo* DFT calculations ($\sim 8^\circ$). Note that for technical reasons the definition of θ_2 is opposite to φ_2 , but the probability ratio of conformers with similar arrangement of the propionic fragment is approximately the same: the conformation with the α -hydrogen opposite to the other substituent of the aromatic system (-F for FLU and -OCH₃ for NAP) turns out to be slightly preferred.

Torsional distribution for the whole molecule. As done for NAP, the rotations around the two dihedral angles θ_1 and θ_2 were assumed to be independent, and the total probability distribution function $P_{iso}(\theta_1, \theta_2)$ to be the product between $P_{iso}(\theta_1)$ and $P_{iso}(\theta_2)$. The definition of the fragment tensors $\varepsilon_{2,p}^j$ for the whole molecule comes from the combination of the interaction tensors defined for the two substructures considered before, fixing in addition $\varepsilon_{C_4,C_7} = \varepsilon_{C_{10},C_{13}}$. Definitely, 7 $\varepsilon_{2,p}^j$ are required: $\varepsilon_{C_4,C_7} = \varepsilon_{C_{10},C_{13}}$, ε_{C_6,C_8} , $\varepsilon_{C_{11},C_{15}}$ and ε_{C_6,F_6} for the biphenyl moiety (*rH+rF*); ε_{C_2,H_2} , ε_{C_2,C_3} and ε_{H_2,C_3} for the *P* fragment.

The whole set of 39 independent D_{ij}^{obs} of Table 2 was then fitted while iterating on the 7 orientational parameters and fixing the 5 conformational terms (θ_1^{max} , θ_2^{max} , A_{θ_2} , h_{θ_1} and h_{θ_2}) at the optimised values found for the single rotations. We obtained a very low RMS error of 0.34 and a good correspondence between D_{ij}^{obs} and D_{ij}^{calc} (reported in Table 2), as it is shown in Figure 5b. The torsional distribution $P_{iso}(\theta_1, \theta_2)$ and the optimised parameters are shown in Figure 8 and Table 7 of ESI. Thanks to the symmetry of the unsubstituted ring, the torsional angle θ_1 was sampled over the 0° - 180° range in order to reduce computational times. Hence, the probability distribution turns out to be characterized by four minimum energy conformers. In agreement with theoretical calculations, the pair of conformers II and IV, having $\theta_1 \sim 44^\circ$ and $\sim 136^\circ$, respectively, and $\theta_2 \sim 188^\circ$, are the most stable with a relative percentage of 57%. The pair of conformers I and III, with $\theta_1 \sim 44^\circ$ and $\sim 136^\circ$, respectively, and $\theta_2 \sim 8^\circ$, are slightly less populated (relative percentage of 43%) and differ in the spatial arrangement of the propionic side chain: as usual for 2-arylpropionic acids the preferred conformation bears the α -hydrogen in opposite position with respect to the other substituent of the aromatic system (-OCH₃ or -F).

Conclusions

The conformational behaviour of *S*-naproxen and *R*-flurbiprofen, two common anti-inflammatory drugs with two non-cooperative internal rotations, has been investigated experimentally in solution by using a combination of NMR in PBLG-based weakly ordering liquid crystals and the AP-DPD theoretical approach.

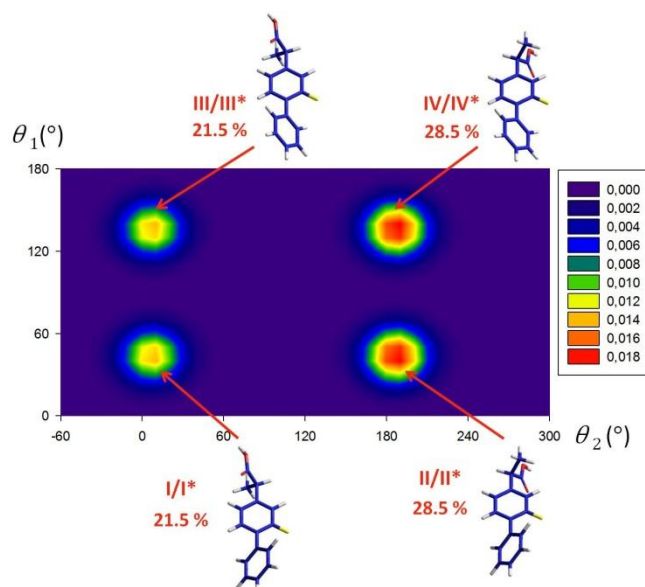


Figure 8. Experimental probability distribution $P_{iso}(\theta_1, \theta_2)$ obtained by AP-DPD approach for *R*-flurbiprofen dissolved in PBLG/THF-*d*₈, including structures of minimum energy conformers and their relative abundance. The surface is obtained by varying θ_1 over the 0° - 180° range and θ_2 over the 0° - 360° range, both with a 10° -step sampling. To better visualize the location of the maxima, θ_2 is plotted from -60° to 300° .

Four minimum energy structures have been found for *S*-naproxen: a couples of more stable conformers (I and II) with the methoxy group in the “*cis*” arrangement ($\varphi_1 \sim 0^\circ$) and a couple of less stable conformers (III and IV) involving the “*trans*” geometry of the same group ($\varphi_1 \sim 180^\circ$). For the fluorinated molecule of *R*-flurbiprofen the fitting procedure of the dipolar couplings set gave a probability distribution characterized by four pairs of symmetry-related conformers. The inter-ring torsion angle was found to be about $\theta_1 \pm 44^\circ$ and $\pm 136^\circ$, in accordance with the results obtained for other *ortho*-fluorinated biphenyl systems.^{53,61} Both the 2-arylpropionic derivatives are characterized by a similar arrangement of the chiral side chain: the preferred conformation adopted by the α -hydrogen is almost coplanar to the aromatic plane and in opposite position with respect to the other substituent of the aromatic system (methoxy group in *S*-naproxen and fluorine atom in *R*-flurbiprofen). These results testify that the use of NMR in weakly ordering PBLG phases makes it possible to achieve a level of accuracy in the description of the drugs’ conformational behaviour that is hardly reached by other standard experimental techniques. The proposed methodology, combining NMR spectroscopy with the use of partially ordered phases, allows, for instance, to overcome the limitations of a conformational analysis by standard nOe measurements.⁶⁵

To achieve such accurate conformational descriptions quite extended data sets of dipolar couplings have been collected, namely 34 and 39 for *S*-naproxen and *R*-flurbiprofen respectively. These large sets can be unambiguously reproduced only considering equilibria among global and local minimum energy conformers, whereas they are not compatible with a model based on a single more populated

conformer. Taking into account a distribution of energetically-admissible conformers is mandatory when searching for a drug's bioactive conformation. As discussed in the Introduction, global minima theoretically calculated *in vacuo* and/or structures experimentally determined by X-ray crystallography do not always well represent the bound conformation of flexible compounds.³¹⁻³⁴ Hence, for a rational structure-based drug design, the exploration of a wide conformational space, including global and local minima possibly present in solution, is of utmost importance. To this end, the strategy adopted in present work represents an effective way for probing the probability distributions of dissolved small to medium-size flexible molecules.

Experimental Details

Two isotropic solutions were obtained by diluting NAP (39.5 mg) in THF-d₈ (519 mg) and FLU (20 mg) in THF-d₈ (525 mg), respectively. The anisotropic samples were prepared by dissolving NAP (41.3 mg) in a liquid-crystalline phase made of PBLG (76.4 mg, DP= 743) and THF-d₈ (393.3 mg) and FLU (30.0 mg) in a liquid-crystalline phase composed of PBLG (104.1 mg, DP = 741) and THF (649.0 mg). All anisotropic samples were prepared using standard procedure described in literature⁵³ and the resulting o.d. 5 mm NMR tubes were centrifuged back and forth until an optically homogeneous birefringent phase was obtained. FLU, NAP and PBLG were purchased from Sigma Aldrich, while THF-d₈ from Eurisotop. All the chemical compounds were used without further purification. For the samples NAP/THF-d₈ and NAP/PBLG/THF-d₈, all the ¹H and ¹³C spectra were recorded at 300 K on a liquid high-resolution Bruker Avance 400MHz spectrometer (9.4 T) equipped with a BBI or QXO probe with a z field-gradient coil. For the samples FLU/THF-d₈ and FLU/PBLG/THF-d₈, the ¹H, ¹⁹F and ¹³C spectra were recorded at 304 K on a liquid high-resolution Bruker Avance 500MHz spectrometer (11.74 T) equipped with TBO and SEF probes. In all cases, temperature was carefully fed-back by a standard variable-temperature unit (BVT-3000).

Acknowledgements

The present work has been supported by the "L'Oréal Italia per le Donne e la Scienza" program through the fellowship of M. E. Di Pietro. Moreover, G. Celebre, G. De Luca and M. E. Di Pietro thank University of Calabria for financial support.

Notes and references

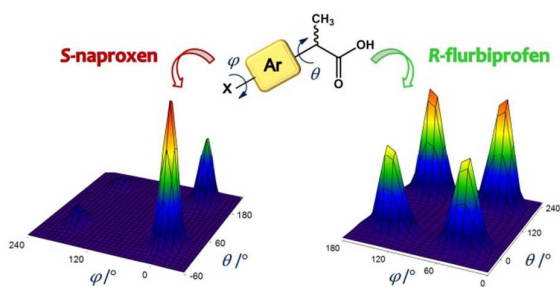
- W. L. Smith, D. L. DeWitt, R. M. Garavito, *Annu. Rev. Biochem.*, 2000, **69**, 145.
- A. L. Blobaum, L. J. Marnett, *J. Med. Chem.*, 2007, **50**, 1425.
- K. D. Rainsford, *Subcell. Biochem.*, 2007, **42**, 3.
- P. J. Hayball, *Drugs*, 1996, **52**, 47.
- M. F. Landoni, A. Soraci, *Curr. Drug Metab.*, 2001, **2**, 37.
- S. S. Adams, P. Bresloff, C. G. Mason, *J. Pharm. Pharmacol.*, 1976, **28**, 256.
- K. C. Duggan, D. J. Hermanson, J. Musee, J. Prusakiewicz, J. L. Scheib, B. D. Carter, S. Banerjee, J. A. Oates, L. J. Marnett, *Nat. Chem. Biol.*, 2011, **7**, 803.
- J. U. Flanagan, Y. Yosaatmadja, R. M. Teague, M. Z. L. Chai, A. P. Turnbull, C. J. Squire, *Plos One*, 2012, **7**, e43965.
- C. Boynton, C. Dick, F. Mayer, *J. Clin. Pharmacol.*, 1988, **28**, 512.
- E. A. MacGregor, *Drugs*, 2010, **70**, 1799.
- V. E. Steele, C. V. Rao, Y. Zhang, J. Patlolla, D. Boring, L. Kopelovich, M. M. Juliana, C. J. Grubbs, R. A. Lubet, *Cancer Prev. Res.*, 2009, **2**, 951.
- E. D. Agdeppa, V. Kepe, A. Petrić, N. Satyamurthy, J. Liu, S.-C. Huang, G. W. Small, G. M. Cole, J. R. Barrio, *Neuroscience*, 2003, **117**, 723.
- B. P. Imbimbo, V. Solfrizzi, F. Panza, *Front. Aging Neurosci.*, 2010, **2**, 1.
- A. P. Roszkowski, W. H. Rooks II, A. J. Tomolins, L. M. Miller, *J. Pharmacol. Exp. Ther.*, 1971, **179**, 114.
- U. A. Boelsterli, H. J. Zimmerman, A. Kretz-Rommel, *Crit. Rev. Toxicol.*, 1995, **25**, 207.
- R. A. Sheldon, *Chirotechnology: industrial synthesis of optically active compounds*, Marcel Dekker, New York, 1993.
- Y. B. Kim, I. Y. Park, W. R. Lah, *Arch. Pharm. Res.*, 1990, **13**, 166.
- Y. B. Kim, H. J. Song, *Arch. Pharm. Res.*, 1984, **7**, 137.
- D. E. Braun, M. Ardid-Candel, E. D'Oria, P. G. Karamertzanis, J.-B. Arlin, A. J. Florence, A. G. Jones, S. L. Price, *Cryst. Growth Des.*, 2011, **11**, 5659.
- R. J. Kulmacz, W. E. Lands, *J. Biol. Chem.*, 1985, **260**, 12572.
- G. Geisslinger, J. Lotsch, S. Menzel, G. Kobal, K. Brune, *Br. J. Clin. Pharmacol.*, 1994, **37**, 392.
- G. Geisslinger, H. G. Schaible, *J. Clin. Pharmacol.*, 1996, **36**, 513.
- J. D. McCracken, W. J. Wechter, Y. Liu, R. L. Chase, D. Kantoci, E. D. Jr. Murray, D. D. Quiggle, Y. Mineyama, *J. Clin. Pharmacol.*, 1996, **36**, 540.
- E. J. Quann, F. Khwaja, K. H. Zavitz, D. Djakiew, *Cancer Res.*, 2007, **67**, 3254.
- W. J. Wechter, D. D. Leipold, E. D. Murray Jr., D. D. Quiggle, J. D. McCracken, R. S. Barrios, N. M. Greenberg, *Cancer Res.*, 2000, **60**, 2203.
- W. J. Wechter, D. D. Leipold, D. D. Quiggle, J. D. McCracken, E. D. Murray, Jr., B. E. Loughman, *Inflammopharmacology*, 2000, **8**, 189.
- G. K. Wilcock, S. E. Black, S. B. Hendrix, K. H. Zavitz, E. A. Swabb, M. A. Laughlin, *Lancet Neurol.*, 2008, **7**, 483.
- J. Boström, *J. Comput. Aided Mol. Des.*, 2001, **15**, 1137.
- E. Perola, P. S. Charifson, *J. Med. Chem.*, 2004, **47**, 2499.
- H. Furukawa, T. Hamada, M. K. Hayashi, T. Haga, Y. Muto, H. Hirota, S. Yokoyama, K. Nagasawa, M. Ishiguro, *Mol. Pharmacol.*, 2002, **62**, 778.
- B. Luy, A. Frank, H. Kessler, in *Molecular Drug Properties. Measurement and Prediction*, ed. R. Mannhold, Wiley-VCH Verlag GmbH & Co. KGaA, Weinheim, 2008, ch. 9, pp. 207-254.
- M. Nicklaus, S. Wang, J. S. Driscoll, G. W. A. Milne, *Bioorg. Med. Chem.*, 1995, **3**, 411.
- G. R. Stockwell, J. M. Thornton, *J. Mol. Biol.*, 2006, **356**, 928.
- A. R. Leach, J. Harren, in *Structure-based drug discovery*, Springer: Berlin, 2007.
- J. W. Emsley, in *Encyclopedia of Magnetic Resonance*, John Wiley & Sons: New York, 2007.
- NMR of Ordered Liquids*, eds. E. E. Burnell, and C. A. de Lange, Kluwer Academic: Dordrecht, The Netherlands, 2003.
- G. Celebre, M. Concistrè, G. De Luca, M. Longeri, G. Pileio, J. W. Emsley, *Chem. Eur. J.*, 2005, **11**, 3599.
- G. Celebre, G. De Luca, M. Longeri, A. Ferrarini, *Mol. Phys.*, 1994, **83**, 309.
- G. Celebre, G. De Luca, M. Longeri, *J. Phys. Chem.*, 1992, **96**, 2466.

- 40 G. Celebre, G. De Luca, M. Longeri, J. W. Emsley, *Mol. Phys.*, 1989, **67**, 239.
- 41 A. Saupe, G. Englert, *Phys. Rev. Lett.*, 1963, **11**, 462.
- 42 E. T. Samulski, A. V. Tobolski, *Macromolecules*, 1968, **1**, 555.
- 43 J. Courtieu, P. Lesot, A. Meddour, D. Merlet, C. Aroulanda, *Encyclopedia of NMR: Advances in NMR*, 2002, **9**, 497.
- 44 C. Aroulanda, V. Boucard, F. Guibé, J. Courtieu, D. Merlet, *Chem. Eur. J.*, 2003, **9**, 4536.
- 45 C. M. Thiele, S. Berger, *Org. Lett.*, 2003, **5**, 705.
- 46 J.-M. Péchiné, A. Meddour, J. Courtieu, *Chem. Commun.*, 2002, 1734.
- 47 M. Rivard, F. Guillen, J.-C. Fiaud, C. Aroulanda, P. Lesot, *Tetrahedron: Asymmetry*, 2003, **14**, 1141.
- 48 P. Lesot, Z. Serhan, I. Billault, *Anal. Bioanal. Chem.*, 2011, **399**, 1187.
- 49 P. Lesot, M. Sarfati, J. Courtieu, *Chem. Eur. J.*, 2003, **9**, 1724.
- 50 P. Lesot, C. Aroulanda, H. Zimmermann, Z. Luz, *Chem. Soc. Rev.*, 2015, **44**, 2330.
- 51 D. O'Hagan, R. J. M. Goss, A. Meddour, J. Courtieu, *J. Am. Chem. Soc.*, 2003, **125**, 379.
- 52 H. Villar, F. Guibé, C. Aroulanda, P. Lesot, *Tetrahedron: Asymmetry*, 2002, **13**, 1465.
- 53 M. E. Di Pietro, C. Aroulanda, D. Merlet, G. Celebre, G. De Luca, *J. Phys. Chem. B*, 2014, **118**, 9007.
- 54 J. W. Emsley, G. R. Luckhurst, C. P. Stockley, *Proc. R. Soc. London, Ser. A*, 1982, **381**, 117.
- 55 G. Celebre, G. De Luca, J. W. Emsley, E. K. Foord, M. Longeri, F. Lucchesini, G. Pileio, *J. Chem. Phys.*, 2003, **118**, 6417.
- 56 T. Fäcke, S. Berger, *J. Magn. Reson. Ser. A*, 1995, **113**, 114.
- 57 M. E. Di Pietro, C. Aroulanda, D. Merlet, *J. Magn. Reson.*, 2013, **234**, 101.
- 58 A. Bax, R. Freeman, *J. Am. Chem. Soc.*, 1982, **104**, 1099.
- 59 J. Farjon, J. P. Baltaze, P. Lesot, D. Merlet, J. Courtieu, *Magn. Reson. Chem.*, 2004, **42**, 594.
- 60 A. Meddour, P. Berdagué, A. Hedli, J. Courtieu, P. Lesot, *J. Am. Chem. Soc.*, 1997, **119**, 4502.
- 61 J. W. Emsley, P. Lesot, A. Lesage, G. De Luca, D. Merlet, G. Pileio, *Phys. Chem. Chem. Phys.*, 2010, **12**, 2895.
- 62 Release 8.0.3 for Windows, Copyright © 2007 Hypercube, Inc for MD calculations; Release 8.0.10 for Windows when conformational search module was used.
- 63 M. J. Frisch, G. W. Trucks, H. B. Schlegel, G. E. Scuseria, M.A. Robb, J. R. Cheeseman, J. A. Montgomery Jr., T. Vreven, K. N. Kudin, J. C. Burant, J. M. Millam, S. S. Iyengar, J. Tomasi, V. Barone, B. Mennucci, M. Cossi, G. Scalmani, N. Rega, G. A. Petersson, H. Nakatsuji, M. Hada, M. Ehara, K. Toyota, R. Fukuda, J. Hasegawa, M. Ishida, T. Nakajima, Y. Honda, O. Kitao, H. Nakai, M. Klene, X. Li, J. E. Knox, H. P. Hratchian, J. B. Cross, C. Adamo, J. Jaramillo, R. Gomperts, R. E. Stratmann, O. Yazyev, A. J. Austin, R. Cammi, C. Pomelli, J. W. Ochterski, P. Y. Ayala, K. Morokuma, G. A. Voth, P. Salvador, J. J. Dannenberg, V. G. Zakrzewski, S. Dapprich, A. D. Daniels, M. C. Strain, O. Farkas, D. K. Malick, A. D. Rabuck, K. Raghavachari, J. B. Foresman, J. V. Ortiz, Q. Cui, A. G. Baboul, S. Clifford, J. Cioslowski, B. B. Stefanov, G. Liu, A. Liashenko, P. Piskorz, I. Komaromi, R. L. Martin, D. J. Fox, T. Keith, M. A. Al-Laham, C. Y. Peng, A. Nanayakkara, M. Challacombe, P. M. W. Gill, B. Johnson, W. Chen, M. W. Wong, C. Gonzalez, J. A. Pople, Gaussian 03 (Revision C.02), Gaussian Inc., Pittsburgh, PA, 2003.
- 64 L. Alvarez-Valtierra, J. W. Young, D. W. Pratt, *Chem. Phys. Lett.*, 2011, **509**, 96.
- 65 E. Bednarek, W. Bocian, J. Cz. Dobrowolski, L. Kozerski, N. Sadlej-Sosnowska, J. Sitkowski, *J. Mol. Struct.*, 2001, **559**, 369.
- 66 T. Troxler, *J. Phys. Chem. A*, 1998, **102**, 4775.
- 67 R. R. Biekofsky, A. B. Pomilio, R. A. Aristegui, R. H. Contreras, *J. Mol. Struct.*, 1995, **344**, 143.
- 68 Y. G. Smeyers, L. Bouniama, N. J. Smeyers, A. Ezzamarty, A. Hernandez-Laguna, C. I. Sainz-Diaz, *Eur. J. Med. Chem.*, 1998, **33**, 103.
- 69 J. R. Yates, S. E. Dobbins, C. J. Pickard, F. Mauri, P. Y. Ghi, R. K. Harris, *Phys. Chem. Chem. Phys.*, 2005, **7**, 1402.
- 70 G. Celebre, G. De Luca, M. Longeri, *Liq. Cryst.*, 2010, **37**, 923.
- 71 G. Pileio, Ph.D. Thesis, Università della Calabria, Italy, 2005.
- 72 J. W. Emsley, G. Celebre, G. De Luca, M. Longeri, F. Lucchesini, *Liq. Cryst.*, 1994, **16**, 1037.
- 73 A. Mazzanti, L. Lunazzi, R. Ruzziconi, S. Spizzichino, M. Schlosser, *Chem. Eur. J.*, 2010, **16**, 9186.

Table of contents

The conformational behavior of naproxen and flurbiprofen in solution by NMR spectroscopy

Maria Enrica Di Pietro, Christie Aroulanda, Giorgio Celebre, Denis Merlet and Giuseppina De Luca



The conformational equilibrium of common anti-inflammatory drugs has been studied experimentally in solution by NMR in weakly ordering PBLG phases.